Journal Name

ARTICLE TYPE

Cite this: DOI: 00.0000/xxxxxxxxxx

Interplay between synthetic conditions and micromorphology in poly(3,4-ethylenedioxythiophene):tosylate (PEDOT:Tos): an atomistic investigation. Electronic Supplementary Information

A. Cappai,[a] A. Antidormi,[a] A. Bosin,[a] D. Galliani,[b‡] D. Narducci,[b‡] and C. Melis[a]

Received Date
Accepted Date

DOI: 00.0000/xxxxxxxxxx

1 DFT calculations

For each polymerization reaction

$$HX_{n-1}H^+ + HXH^+ + B + B' \rightleftharpoons HX_nH + BH^+ + B'H^+$$

(where B and B' are the proton scavengers), we estimate the Gibbs free energy of reaction $\Delta G(n)$ (where n is the number of monomers composing the oligomer) using a different combination of molecules as proton scavengers. All the calculations are performed both in solution and in vacuo using the Gaussian16 suite of programs[1]. In order to calculate gas phase Gibbs free energies ΔG^0 all the geometries were first optimized at the B3LYP/6-311G(d,p) level and a vibrational frequencies calculation was then performed at the same theory level. The same procedure was employed to estimate the Gibbs free energies in solution G by using the SMD implicit solvent model[2].
Specifically, the Gibbs free energy of reaction is calculated as:

$$\Delta G = \Delta G^0 + \Delta G^{0\rightarrow *} + \Delta G_{\mathrm{sol}} \quad (1)$$

where

- ΔG^0 is the gas-phase Gibbs free energy of reaction;
- $\Delta G^{0\rightarrow *}$ is the Gibbs free energy of transfer from the gas phase to the solution[3]

$$\Delta G^{0\rightarrow *} = \Delta nRT \ln\left(\frac{RT}{pV^*}\right) \quad (2)$$

where Δn is the difference between the sum of moles of products and the sum of moles of reactants, p is the gas phase pressure (1 atm, in the present case), $1/V^*$ is the solute concentration (assumed to be 1 mol/L), T the absolute temperature and R is the gas constant.

- ΔG_{sol} is the solvatation Gibbs free energy accounting for solute-solvent interactions for each reactant and product.

The first and the last terms in Eq. (1) are estimated as the difference between the sum of Gibbs free energies of the products and that of the reactants. The gas-phase Gibbs free energies are calculated by performing an analysis of the vibrational frequencies whereas the SMD implicit solvent model has been employed to compute the solvatation energies. In detail, the Integral equation formalism is implemented in polarizable continuum model (IEFPCM) by taking the electrostatic and non-electrostatic terms (cavitation, dispersion and repulsion energies) from Truhlar and coworkers' SMD solvation model[2].

To assess the accuracy of the present methodology, we calculated the enthalpy and the entropy variations $\Delta H^{\mathrm{theo}}_{298}$ and $\Delta S^{\mathrm{theo}}_{298}$ at T=298 K calculated using the B3LYP functional and the aug-cc-pVDZ basis set[4] for the dissociation reaction of several strong acids. The results are shown in Table 1 together with the corresponding experimental values $\Delta H^{\mathrm{exp}}_{298}$ and $\Delta S^{\mathrm{exp}}_{298}$[4]. In both cases we observe a very good agreement between our calculations and the previous experimental and theoretical data. Finally, a second set of calculations has been carried out to establish the accuracy of the implicit solvent model described via the IEFPCM. We considered the following reaction involving pyridine in solvent water as a reference case:

$$Pyr + H^+ \rightleftharpoons PyrH^+ \quad (3)$$

The calculated value of the Gibbs free energy of reaction is $\Delta G = -8.8074$ kcal mol^{-1}, given by the sum of the three contributions of Eq. (1): in particular, $\Delta G^0 = -910.66$ kcal mol^{-1}, whereas ΔG^0 for an isolated H^+ was analytically estimated by Sackur-Tetodre formula. Importantly, the computed value of ΔG^{theo} is

[a] Department of Physics, Univ. of Cagliari, Cittadella Universitaria, 09042 Monserrato, Italy
[b] Department of Material Science, Univ. of Milano-Bicocca, 20125 Milano, Italy

Table 1 Comparison between the computed dissociation enthalpy $\Delta H_{298}^{\text{theo}}$ and entropy $\Delta S_{298}^{\text{theo}}$ with the corresponding experimental values. Enthalpies are expressed in kcal/mol while entropies are in cal/mol/K.

Species	$\Delta H_{298}^{\text{theo}}$	$\Delta H_{298}^{\text{exp}}$	$\Delta S_{298}^{\text{theo}}$	$\Delta S_{298}^{\text{exp}}$
HBr	324.91	323.5	47	47.425
HCl	329.53	333.4	45	44.605
HI	316.68	314.3	49	49.444
H-HSO_4	313.86	312.5	74	72.725
TfOH	303.75	305.4	89	88.23
TosH	320.08	—	104	99.474

in good agreement with the experimental one, $\Delta G^{\text{exp}} = -7.0449$ kcal/mol[5].

1.1 Classical molecular dynamics

In order to investigate the effect of the proton scavenger over the morphology of PEDOT samples, we developed a novel computational tool to model the PEDOT polymerization, which allows to reproduce *in silico* the chemical processes leading from monomeric units to a polymerized sample. In the present approach molecular dynamics (MD) simulations are blended with first-principle free energy calculations (see previous section), so as to generate a fully atomistic modelling of polymerization. MD takes charge of the dynamical evolution of the system for very long time periods whereas first-principle calculations are exploited to describe (in a probabilistic approach) the oxidative elongation processes. Specifically, the polymerization algorithm consists of two mains steps, which are iteratively repeated until the polymerized sample has been achieved: the dynamical step and the coupling step.

1. **The Dynamical step**
   The first step is responsible for the dynamical evolution of the individual EDOT monomers in the system. In all the MD runs, the positions and velocities of the interacting components are evolved according to Newton's equations of motion, as implemented in the LAMMPS molecular dynamics package[6]. The interatomic interactions are described using the AMBER force field[7], including bonding terms (bonds, angles, and dihedrals) as well as nonbonding contributions (Coulomb and van der Waals). The parameters occurring in the bonding and Van der Waals terms are taken from the GAFF database[8]. The atomic partial charges are estimated with the restrained electrostatic potential (RESP) method[9] as implemented in the Gaussian package. **The velocity-Verlet algorithm with a time step of 0.5 fs is used to solve the equations of motion. A particle-particle particle mesh solver is used for describing the long-range electrostatic forces, and the van der Waals interaction are cut off at 1.0 nm.** The Nosé-Hoover thermostat and barostat with corresponding relaxation time equal to 50 fs and 0.5 ps respectively are used.

2. **The Coupling step**
   The formation of a chemical bond between two EDOT monomers (or one EDOT monomer and one PEDOT oligomer, see Fig. 1) is accomplished in this step adopting a Markov-based approach. To this aim, we introduce a "bond creation probability" p, defined as the probability that two units can bond together forming a larger oligomer. At each time step, the distance between any pair of units is checked if smaller than a given threshold (3 Å in our case), the chemical bond is formed according to the probability p. The corresponding terms in the classical interaction potential are then eventually updated with the introduction of new bonds, angles and dihedrals. Once this step has been performed, the procedure continues with a new iteration of the dynamical step.
   In our model, we assume that different probability values p correspond to different chemical reactions according to the formula

$$p = \min(1, \exp(\Delta G/(K_{\text{B}}T)) \tag{4}$$

   where K_{B} is the Boltzmann constant, T is the temperature and ΔG is the Gibbs free reaction energy. The bond is then formed with probability 1 if the corresponding reaction is energetically favourable ($\Delta G < 0$), otherwise it is created with a probability proportional to the Boltzmann weight.

1.2 Sample preparation

To demonstrate the capabilities of our computational tool, we emulated the polymerization process of systems as large as a cube of side 11.8 nm, containing an initial number of 10,000 EDOT monomeric units. Overall the simulation cell contained as many as 130,000 atoms. The solvent as well as the proton scavengers and tosylate molecules were not present in the simulation cell since their effect has been taken into account in the $\Delta G(n)$ calculations and therefore in the bond creation probabilities. The simulation of the polymerization process required a multi-step procedure to be performed: i) first, the monomers are placed in an initial arbitrary volume in a random fashion; ii) the system is fully relaxed at constant temperature $T = 300$ K and fixed ambient pressure using a Nosé-Hoover thermostat in order to reach the equilibrium values of volume and density; iii) the polymerization algorithm is then finally implemented keeping the temperature constant ($T = 300$ K).

1.3 Sample crystallinity

To quantify the crystallinity of our samples, we calculated the fraction of volume v_{C} occupied by the crystallites. The definition of this quantity relies on the calculation of the local spatial correlation of the orientation of EDOT monomers, $C(\vec{r})$. Specifically, each EDOT unit was labeled with a vector $\vec{s}_i$ joining two carbon atoms in the thiophene ring (see Fig. 1). For each vector $\vec{s}_i$ the spatial correlation reads

$$C(\vec{r}) = \frac{1}{N} \sum_{|\vec{r}-\vec{r}_j|<r_0} |\vec{s}_i(\vec{r}) \cdot \vec{s}_j(\vec{r}_j)| \tag{5}$$

where $\vec{r}$ is the position of the first carbon atom and N is the total number of EDOT monomers. The value of r_0 was set to 5 Å .

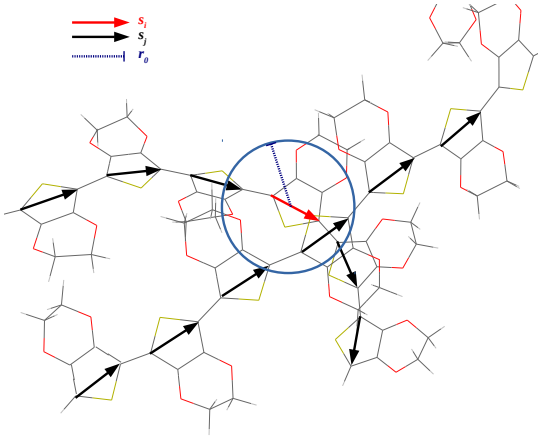

Fig. 1 Schematic representation of the orientation vectors $\vec{s_i}$ and $\vec{s_j}$ used to estimate the spatial local correlation $C(\vec{r})$

Thus, the higher is the correlation between the EDOT monomers orientations (higher values of $C(\vec{r})$), the higher is the local sample crystallinity. Therefore, by mapping the $C(\vec{r})$ values, one identifies the regions of higher crystallinity and the fraction of the sample volume occupied by crystallites v_C. $C(\vec{r})$ ranges from a minimum value of 1e-4, which characterizes samples still not polymerized, up to a maximum value of 5e-3 obtained for a perfect crystalline sample generated as reported in [10]. For our polymerized samples, $C(\vec{r})$ ranges from 1e-4 to 9e-4. $C(\vec{r})$ is large at small distances (where the monomer orientations are strongly correlated), but it rapidly decreases for larger distances. In the latter situation, the monomer orientations become almost uncorrelated.

From the knowledge of $C(\vec{r})$, the volume fraction occupied by crystalline regions v_C has been calculated by estimating the volume of the simulation cell for which $C(\vec{r})$ is larger than a given threshold value $C_{\min}$, i. e.:

$$v_C = \frac{\int_{C(\vec{r})>C_{\min}} \mathrm{d}V}{V_{\text{cell}}} \tag{6}$$

We set $C_{\min} = 0.006$ at about half of the span of values taken by $C(\vec{r})$. Visual inspection of the simulation output further confirmed that the threshold set is the lowest value of C for which stacking is still observed.

Notes and references

1 M. J. Frisch, G. W. Trucks, H. B. Schlegel, G. E. Scuseria, M. A. Robb, J. R. Cheeseman, G. Scalmani, V. Barone, G. A. Petersson, H. Nakatsuji, X. Li, M. Caricato, A. V. Marenich, J. Bloino, B. G. Janesko, R. Gomperts, B. Mennucci, H. P. Hratchian, J. V. Ortiz, A. F. Izmaylov, J. L. Sonnenberg, D. Williams-Young, F. Ding, F. Lipparini, F. Egidi, J. Goings, B. Peng, A. Petrone, T. Henderson, D. Ranasinghe, V. G. Zakrzewski, J. Gao, N. Rega, G. Zheng, W. Liang, M. Hada, M. Ehara, K. Toyota, R. Fukuda, J. Hasegawa, M. Ishida, T. Nakajima, Y. Honda, O. Kitao, H. Nakai, T. Vreven, K. Throssell, J. A. Montgomery, Jr., J. E. Peralta, F. Ogliaro, M. J. Bearpark, J. J. Heyd, E. N. Brothers, K. N. Kudin, V. N. Staroverov, T. A. Keith, R. Kobayashi, J. Normand, K. Raghavachari, A. P. Rendell, J. C. Burant, S. S. Iyengar, J. Tomasi, M. Cossi, J. M. Millam, M. Klene, C. Adamo, R. Cammi, J. W. Ochterski, R. L. Martin, K. Morokuma, O. Farkas, J. B. Foresman and D. J. Fox, *Gaussian~16 Revision B.01*, 2016, Gaussian Inc. Wallingford CT.

2 A. V. Marenich, C. J. Cramer and D. G. Truhlar, *The Journal of Physical Chemistry B*, 2009, **113**, 6378–6396.

3 G. C. Shields and P. G. Seybold, *Computational approaches for the prediction of pKa values*, CRC Press, 2010.

4 K. E. Gutowski, J. D. Holbrey, R. D. Rogers and D. A. Dixon, *The Journal of Physical Chemistry B*, 2005, **109**, 23196–23208.

5 L. Sacconi, P. Paoletti and M. Ciampolini, *Journal of the American Chemical Society*, 1960, **82**, 3831–3833.

6 S. Plimpton, *Journal of computational physics*, 1995, **117**, 1–19.

7 J. W. Ponder and D. A. Case, in *Advances in protein chemistry*, Elsevier, 2003, vol. 66, pp. 27–85.

8 J. Wang, R. M. Wolf, J. W. Caldwell, P. A. Kollman and D. A. Case, *Journal of computational chemistry*, 2004, **25**, 1157–1174.

9 C. I. Bayly, P. Cieplak, W. Cornell and P. A. Kollman, *The Journal of Physical Chemistry*, 1993, **97**, 10269–10280.

10 C. Genovese, A. Antidormi, R. Dettori, C. Caddeo, A. Mattoni, L. Colombo and C. Melis, *Journal of Physics D: Applied Physics*, 2017, **50**, 494002.